Soft Matter

Small-volume extensional rheology of concentrated protein and protein-excipient solutions

Journal:	*Soft Matter*
Manuscript ID	SM-ART-08-2021-001253.R1
Article Type:	Paper
Date Submitted by the Author:	29-Sep-2021
Complete List of Authors:	Lauser, Kathleen; University of Minnesota System, Chemical Engineering and Materials Science Rueter, Amy; University of Minnesota System, Chemical Engineering and Materials Science Calabrese, Michelle; University of Minnesota System, Chemical Engineering and Materials Science

Soft Matter

ARTICLE TYPE

Cite this: DOI: 00.0000/xxxxxxxxxx

Small-volume extensional rheology of concentrated protein and protein-excipient solutions†

Kathleen T. Lauser, Amy L. Rueter, and Michelle A. Calabrese*

Received Date
Accepted Date

DOI: 00.0000/xxxxxxxxxx

Limited studies measure extensional rheology in protein solutions due to volume constraints and measurement challenges. We developed a small-volume, Dripping-onto-Substrate (DoS) extensional rheology device to measure the capillary thinning of protein and protein-excipient solutions via DoS for the first time. Ovalbumin (OVA) was used as a model system, examined via DoS both with and without excipient poloxamer 188 (P188). Water and dilute OVA break apart rapidly and demonstrate inertiocapillary (IC) thinning behavior, where longer breakup times in OVA can be attributed to lower surface tension. Further increasing OVA content leads to longer breakup times and deviations from IC thinning at the start of thinning, however, no evidence of elastic behavior is observed. P188 more effectively lowers the droplet surface tension than OVA, transitioning from IC behavior in dilute solution to weakly elastic behavior at higher concentrations. Combined protein/excipient formulations act synergistically at low concentrations, where breakup times are identical to those of the individual components despite the higher total concentration. However concentrated protein/excipient formulations exhibit elasticity, where extensional rheology parameters depend on P188 content and total concentration. These findings imply that excipients intended to stabilize proteins in shear flow can cause undesirable behavior in extensional flows like injection.

1 Introduction

Solution-based protein therapeutics, such as insulin or monoclonal antibodies (mAbs), are important novel treatments for complex diseases including cancer, infectious and autoimmune diseases, and allergies, with global sales of over $288 billion in 2016.[1,2] These therapeutics, often administered via intravenous injection, are orders of magnitude larger than small molecule drugs, have complex secondary and tertiary structures, and are difficult to produce. Unsurprisingly, the size and complexity of these and cellular therapeutics cause substantial challenges in development, delivery and stability.[3–6] New protein therapeutics are screened based on their stability and viscosity at rest, largely dictated by concentration and interactions between proteins.[7] However, these metrics are not indicative of stability during injection flows[4] which contain strong shear and extensional forces that accelerate protein aggregation and denaturing, subsequently reducing clinical efficiency and antibody response.[8] Additional FDA guidelines on injection viscosity and volume have led to administration via dilute, low viscosity intravenous injections, which require long, expensive hospital treatments.[7,9,10]

Delivery via rapid intravenous injection or subcutaneous injection would reduce the burden on the healthcare system,[7,9–11] but requires small volume, concentrated formulations and smaller needles, which increase shear and extensional deformation rates.[8,10] Thus accurately measuring therapeutic flow properties during extensional flows is necessary to develop flow-stable concentrated therapeutics with minimal adverse interactions between formulation components, thereby improving patient safety and access to treatment while reducing healthcare costs. However, accurately measuring protein rheology is complicated, as air-liquid and solid-liquid interfaces substantially affect the measurement due to aggregation at these interfaces driven by differences in interfacial tension.[12–14] Proteins, like surfactants and polymers, migrate to droplet interfaces and aggregate, thus reducing the surface tension of the droplet. In shear rheology, this aggregation can cause film formation which dominates the torque signal and extracted rheological parameters, often on a timescale of hours[5,13–20]; thus many studies of proteins in shear flow are incomplete or inconclusive.

Adding stabilizing surfactant excipients is one route to reduce the aggregation and resulting shear viscosity, though protein-excipient interactions during extensional flows are not well understood. Recently, Rodrigues et. al examined the rheological properties of concentrated protein/excipient formulations, noting that excipients added to enhance protein solution stability are

421 Washington Ave SE, Minneapolis, MN 55455 Fax: 612-626-724; Tel: 612-625-1313

*Corresponding author, Email: Michelle Calabrese, mcalab@umn.edu

† Electronic Supplementary Information (ESI) available: [details of any supplementary information available should be included here]. See DOI: 10.1039/cXsm00000x/

typically evaluated at low protein concentration.[21] The authors show that a crowded solution environment may significantly impact protein/excipient interactions, increasing viscosity and aggregation. However here, only the shear viscosity of concentrated protein/excipient formulations was examined, which may not accurately represent extensional rheological properties.

The extensional flow of protein solutions is even more sparsely studied than shear due to experimental limitations.[22] While stretching a solid is trivial, no simple equivalence for gripping and stretching a fluid exists. Unlike in shear rheology, extensional rheology requires sample re-loading after each test, necessitating large protein volumes. Finally, most extensional flow devices produce mixed shear and extensional flows, cover limited extension rates, or are not commercially available.[5,23,24] Limited experimental studies on proteins in extensional flow primarily focus on dilute, nearly Newtonian solutions in microfluidic devices.[25–28] Elongational flow was shown to cause aggregation, unfolding, and fiber formation, the degree to which depends on protein size, pH, concentration and sequence.[26–29] However, few of these studies extracted fundamental rheological parameters like extensional viscosity and relaxation time, or processing parameters like droplet break-up time, which are required to understand and predict protein stability and to meet FDA guidelines.[5,9–11]

The limited studies to extract rheological parameters demonstrate the need for additional tools to measure protein extensional rheology. Hosseini and co-workers observed elastic thinning behavior in dilute tau proteins (10 mg/mL) using a modified tensiometer for liquid bridge generation; extracted viscoelastic relaxation times were similar in magnitude to those for dilute polyethylene oxide (PEO) solutions.[29] Brust et al. showed that dilute bovine serum albumin (BSA) solutions are Newtownian in both shear and extensional rheology experiments. However, the authors found that while blood and blood plasma exhibit Newtonian behavior in shear, pronounced elasticity is observed in extension, with extensional relaxation times comparable to those observed in viscoelastic PEO controls.[22] Based on the flow regimes occurring prior to the observed elasticity and the rapid capillary thinning timescales (typically ms), these works could eliminate the presence of a protein interfacial film as a substantial contributor to the measured rheology. The appearance of viscoelastic behavior in protein solutions during extension that is undetectable in shear further motivates accurate extensional rheology measurements on concentrated protein therapeutics, which are more likely to be non-Newtonian than their dilute counterparts.[30,31]

Capillary-driven thinning of a liquid bridge can be used to measure extensional rheology (Fig. 1), as no active external forces are present during break-up.[24,32] Liquid bridge thinning is mathematically described by distinct behavioral regimes accounting for inertial, viscous, elastic, and capillary forces. Here, the dimensionless Ohnesorge number quantifies viscous forces to inertial and surface tension forces and dictates the dominant flow regime:

$$Oh = \frac{\mu}{\sqrt{\rho \sigma R_0}} \tag{1}$$

where μ, ρ, σ and R_0 are the dynamic viscosity, density, surface tension and outer radius of the nozzle respectively.[24,32,33] Extensional rheology parameters and timescales are then determined by fitting the temporal decay of the fluid filament radius. For example, when $Oh < 1$, inertial and surface tension forces dominate, known as inertiocapillary (IC) thinning; viscocapillary (VC) thinning occurs when $Oh > 1$. While commercial instruments like the Capillary Breakup Extensional Rheometer (CaBER) can measure capillary thinning in complex fluids, these instruments apply a step strain via plate separation to form the liquid bridge. Unfortunately, this step strain causes pre-deformation that can impact extracted rheological parameters and excludes measuring low viscosity fluids like proteins because the thinning timescale is similar to that for plate separation.[23,32,34]

Dripping-onto-Substrate (DoS) rheology, originally pioneered by Dinic and Sharma,[32,35] allows access to a wider range of extension rates, viscosities and concentrations and generates minimal pre-deformation when compared to CaBER.[32,36–38] DoS devices employ a syringe pump at a low flowrate to create a single hemispherical drop, which makes contact with a substrate to form the liquid bridge.[35] The time-dependent dimensions of the liquid bridge are recorded by a high-speed camera; images are then processed to obtain radial decay profiles and extract rheological properties. While DoS is most commonly used to examine viscoelastic polymer solutions,[32,39,40] the technique has also been used for fluids like water and glycerol,[35] surfactant solutions,[41] and particle suspensions.[42,43] The range of accessible viscosities and flow regimes makes this technique ideal for studying of a wide concentration range of protein solutions, which may exhibit inertiocapillary through elastic behavior.[22]

Herein, we develop and validate a direct-mount DoS instrument to measure the extensional flow behavior of dilute and concentrated protein solutions via DoS for the first time. The direct mount approach enables a substantial reduction in sample volume, which is required due to scarcity of protein material and cost, such that each measurement requires less than 10 μL total. We then demonstrate the impact of increasing protein concentration on the extensional flow behavior and observed flow regimes in ovalbumin (OVA) solutions. OVA was chosen as a model protein similar in size (44.3 kDa) to the globular insulin hexamer (36 kDa). Though most protein therapeutics are larger than 100 kDa and extensional flow effects generally increase with molecular weight, insulin can lose reliability and efficacy depending on the delivery method,[3,8] motivating study of model proteins substantially smaller than 100 kDa. Finally, we examine the effect of adding FDA-approved excipient poloxamer 188 (P188), commonly used to impede protein aggregation under shear flows or at rest,[44–46] on the extensional flow properties of OVA solutions.

2 Materials and Methods

2.1 Materials

OVA was obtained from Sigma Aldrich (globular, 42 kDa peptide portion only, 44.3 kDa total, lyophilized powder, >98%) and used as received. Kolliphor P188 ($M_n = 8.4$ kDa, also known by F68), a commonly used poloxamer excipient,[1,21,47–49] was obtained from Sigma Aldrich and used as received. Polyethylene oxide (PEO, M_W = 1,000 kDa) used for device validation was obtained from

Beantown Chemical and used as received.

Optically clear OVA solutions were prepared by dissolving OVA into DI water and kept at pH 7 based on prior protocols.[50] OVA solutions were placed on a refrigerated orbital shaker for several hours to ensure full dissolution. Protein samples were typically measured within 24 hours of preparation, and at maximum, within one week of preparation to avoid bacterial contamination and to eliminate well-documented protein degradation pathways related to excipient impurities.[51] Aqueous P188 solutions were placed on a refrigerated orbital shaker for a minimum of eight hours before use; all solutions were optically clear. Combined OVA and P188 solutions were created by dissolving OVA into pre-made P188 solutions in mass ratios of 2:1, 1:1, and 1:2 OVA:P188, keeping similar ratios as previous works.[47,52–54] PEO solutions were prepared by shaking on a room temperature orbital shaker for 2-5 days until all white powder was dissolved.

2.2 Sample characterization

Sodium dodecyl sulfate–polyacrylamide gel electrophoresis (SDS-PAGE) was performed to verify protein identity and purity by following Laemmeli's method,[55] using a Bio-Rad mini-Protean Tetra and Blotting module and a Thermo Scientific PageRuler Plus Prestained Protein Ladder. The running buffer, gel fixing buffer, and destain solution were 10x Tris/Glycine/SDS, 50% ethanol/10% acetic acid in water, and 50% methanol/10% acetic acid in water, respectively. Gels were stained using 0.1% wt Coomassie blue G-250 (Sigma-Aldrich) with 20% methanol and 10% acetic acid in water, and were visualized using a Bio-Rad ChemiDoc Touch imaging system. Bio-Rad ImageLab version 6.1 software was used for quantification of the bands. See SI.2 for gel images and analysis.

Dynamic light scattering (DLS) experiments were performed with a Wyatt Dynopro plate reader equipped with a 830 nm laser at 25 °C. Measurements were performed in triplicate, with at least 5 individual runs of 10 s acquisition time averaged together per trial. Data was analyzed using Wyatt DYNAMICS software V7.10. DLS was performed on dilute OVA solutions (1 mg/mL) to confirm the expected hydrodynamic radius, R_h.[56,57] Measurements were also performed at several concentrations of P188 to confirm the presence of unimers or micelles (see SI.5).

2.3 Low volume dripping-onto-substrate (DoS) device

The dripping-onto-substrate device was constructed in-house following previous work by Dinic and co-workers,[32] and modified to conserve volume (Fig. 1). Major device components include lighting, camera, and dispensing system. Briefly, a 2600 lumen cool white bulb behind a diffuser screen illuminates the droplet. A Chronos 1.4 high-speed camera (38,000 fps max) records videos, typically between 2,000 to 12,000 frames per second (fps) to balance temporal and spatial resolution. Raw images are converted to binary with ImageJ[58] and then to a matrix of normalized radii in time and space, which is fit to the appropriate model equation based on *Oh* and visual evidence from filament thinning shapes (see Results and Discussion for more details). To minimize volume compared other designs,[32] a syringe pump with low flowrate dispensing capabilities ($\geq$0.1 μL/h) was mounted directly to the wall to eliminate excess tubing. An 18 gauge nozzle (ID=0.84 $\pm$ 0.01 mm, OD=1.27 $\pm$ 0.01 mm) and a 250 μL syringe are used to create the droplet. A clean glass slide is used as a partially wetting substrate (θ <90°) to separate the thinning process from droplet spreading dynamics.[32] The contact angle for all trials was <80°; results were independent of contact angle in this range (see SI.4). The slide sits on an adjustable stage (Toauto, XYZ manual linear stage), which rests on anti-vibration pads. The standard configuration has an aspect ratio, $h/2R_0$, between two and three, with $2R_0 = 1.27$ mm.

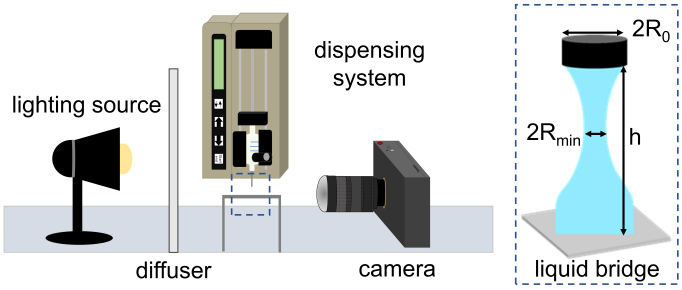

Fig. 1 Schematic of the direct-mount dripping-onto-substrate device. A high-speed camera records thinning of the liquid bridge with radius R_{min}, backlit using a diffused bright light. The liquid bridge is formed from a single drop, produced by a syringe pump directly mounted to the wall.

One consequence of the direct-mount approach is that pump vibrations which are typically minimized by addition of tubing between the syringe pump and droplet outlet[32,35] now cause small vibrations in the droplet, particularly as the droplet grows; these vibrations could highly impact measurements of low viscosity or low elasticity fluids. Thus to minimize this pre-deformation, the pump is stopped prior to the drop contacting the substrate. The stage, which can be moved in 10 μm increments, is slowly moved up to contact the droplet. This procedure is different than that used in prior work,[32,35] which used a low flow rate from a syringe pump to make contact with the substrate. However, our 'stationary drop' method enabled a straight liquid bridge to be formed via the direct-mount approach without accompanying vibrations. Note that added tubing requires milliliter or larger sample volumes that are impractical for measuring proteins.

2.4 Surface tension measurements

Stopping the pump prior to the drop contacting the substrate also enables a stable pendant drop to form prior to thinning, in which drop shape analysis can be used to extract the surface tension, σ. Pendant drop profiles are analyzed via automated algorithms based on the Laplace equation using an ImageJ pendant drop plug-in[59]; this process was first validated with water of known surface tension. The surface tension value for water extracted using this method was 74.1 $\pm$ 1.9 mN/m at 95% confidence (Table 1), compared to a literature value of 72.7 mN/m at 20 °C.[60]

2.5 Validating direct mount DoS with model PEO solutions

Aqueous polyethylene oxide (PEO) solutions were used for device validation, as PEO exhibits three major regimes of extensional thinning behavior: inertio-capillary (IC), visco-capillary (VC),

and elasto-capillary (EC) thinning.[32] These well-defined regimes are documented with both DoS and CaBER,[32,61,62] making PEO an ideal validation material. Representative data on 0.5% wt PEO from our device and Dinic et al.[63] is shown in Fig. 2.

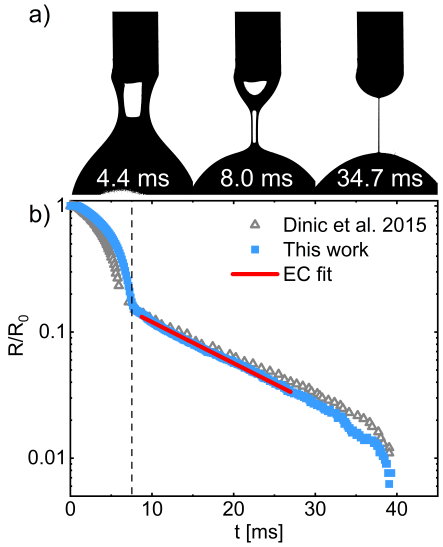

Fig. 2 a) Images of filament thinning at three timepoints in 0.5% wt aqueous PEO, and b) extracted radial decay curve (■). b) The dashed line marks a transition between IC and EC regimes, the latter of which is fit with Eq. 2 to obtain a relaxation time, λ_E. Radial thinning profiles and λ_E compare favorably with Dinic et al. (digitized △).[63]

As seen from the high-speed images (Fig. 2a), PEO forms an axisymmetric cylindrical liquid bridge. After an initial IC region,[63] a pronounced transition to elastocapillary thinning occurs where the filament radius decreases exponentially in time (Fig. 2b). The EC region thus appears as a linear region in the radial decay data on a semilog scale in Fig. 2b. For polymer solutions that can be described reasonably well by a single relaxation time, the data in the EC region can be fit to extract the extensional relaxation time, λ_E, by the following approximation:[64,65]

$$\frac{R_{min}(t)}{R_0} \approx \left(\frac{GR_0}{2\sigma}\right)^{1/3} \exp(-t/3\lambda_E) \qquad (2)$$

where R_{min} is the minimum radius and G is the elastic modulus.

Fits to Eq. 2 yield extensional relaxation times, λ_E, for our instrument of 4.02 ± 0.18 ms; note that $\left(\frac{GR_0}{2\sigma}\right)^{1/3}$ is treated as a fitting constant, as is typically done.[32,66] These λ_E values compare favorably to Dinic[63] (λ_E=4.66 ± 0.23 ms) despite differences in polymer batch and supplier. Additionally, no evidence of vibrations or surface instabilities are seen in DoS videos or in the 1D radial decay curves for PEO or other dilute solutions, confirming the validity of the direct mount, stationary drop approach. See Supporting Information for representative videos for samples used in this work, SI.3 for additional PEO validation data, and SI.9 for 1D data for all water, protein, and excipient trials.

3 Results and discussion

3.1 Capillary thinning of OVA with increasing concentration

The role of protein concentration on the capillary thinning of ovalbumin solutions was explored at three OVA loadings: 100, 200, and 300 mg/mL (denoted OVA100, OVA200, and OVA300, respectively). Water was also measured as a control with known inertiocapillary (IC) behavior. To aid in interpreting the flow behavior of each sample, surface tension measurements were taken prior to thinning, since surface forces are critical in driving capillary thinning and determining *Oh*. With initial OVA addition, σ greatly decreases, where $\sigma = 74.1 \pm 1.9$ mN/m for water versus $\sigma = 47.5 \pm 1.3$ mN/m for OVA100 (Table 1). This large initial drop in σ is due to the presence of OVA at the air-water interface. Subsequent OVA addition further decreases σ but to a lower degree, likely due to interface saturation, where $\sigma = 42.1 \pm 1.2$ mN/m and 41.7 ± 1.1 mN/m for OVA200 and OVA300, respectively.

Capillary thinning measurements show that the break up time, t_b, increases with concentration and decreasing surface tension, where t_b = 3.3 ± 0.1 ms, 4.4 ± 0.3 ms, 6.1 ± 0.4 ms, and 10.1 ± 0.9 ms for water, OVA100, OVA200 and OVA300, respectively (Table 1, Fig. 3b). In Table 1, reported parameter uncertainties are the 95% confidence interval around the parameter based on multiple trials ($N \geq 5$); for raw data on all trials and reproducibility, see SI.9. As seen in the 2D images during thinning shown in Fig. 3a, the liquid bridge in the water control exhibits a conical shape, as is characteristic for inviscid pinchoff.[67–69] With increasing OVA concentration, the shape of the liquid bridge at equivalent non-dimensional radii (R/R_0) transitions from conical to more cylindrical. The liquid bridge in OVA100 is most similar in shape to the water control in the final frame prior to breakup; however, the 2D images during thinning show that OVA thinning

Table 1 DoS samples with measured surface tension σ, calculated and fit constant C and Rayleigh time t_R, breakup time t_b, and initial and final thinning indices, n_0 and n. Reported uncertainty is the 95% confidence interval of the parameter value based on fits to all trials (see SI.9 for all raw data). Uncertainties for C_{calc}, $t_{R,calc}$, and for $t_{R,fit}$ values marked by † are of order 0.01. ** values indicate samples exhibiting weakly elastic behavior (strong deviations from IC). Only n is fit for water due to limited points in the fitting regime.

sample	σ [mN/m]	C_{calc}	C_{fit}	$t_{R,calc}$ [ms]	$t_{R,fit}$ [ms]	t_b [ms]	n_0	n
water	74.1 ± 1.9	39.7	40.1± 2.8	1.9	1.8 ± 0.1	3.3 ± 0.1	N/A	0.64± 0.02
OVA100	47.5 ± 1.3	34.2	34.3 ± 4.6	2.3	2.3 ± 0.1	4.4 ± 0.3	0.64 ± 0.02	0.64 ± 0.02
OVA200	42.1 ± 1.2	32.9	31.2 ± 2.0	2.5	2.7†	6.1 ± 0.4	0.62 ± 0.01	0.64 ± 0.02
OVA300	41.7 ± 1.1	32.8	27.9 ± 2.4	2.5	3.2 ± 0.1	10.1 ± 0.9	0.50 ± 0.01	0.63 ± 0.03
P188-50	43.2 ± 0.7	33.1	30.1 ± 3.2	2.4	2.8 ± 0.1	4.6 ± 0.1	0.62± 0.01	0.63± 0.02
P188-100	41.4 ± 0.4	32.7	29.2 ± 2.0	2.5	2.9 ± 0.1	5.8 ± 0.5	0.62 ± 0.01	0.65 ± 0.02
P188-200	41.8 ± 1.0	32.8	37.2 ± 1.4**	2.5	2.0†**	9.6 ± 0.5	0.61 ± 0.04	0.77 ± 0.02**
OVA100/P188-50	42.8 ± 1.5	33.1	34.1 ± 2.7	2.4	2.3 ± 0.1	4.9 ± 0.3	0.64 ± 0.02	0.66 ± 0.02
OVA100/P188-100	42.1 ± 0.8	32.9	26.3 ± 3.1	2.5	3.4 ± 0.1	7.3 ± 0.3	0.58 ± 0.02	0.65 ±0.02
OVA100/P188-200	37.7 ± 2.0	31.7	120.3 ± 9.3**	2.6	0.4 ± 0.1**	14.9 ± 1.3	0.56 ± 0.03	0.99 ± 0.03**
OVA200/P188-100	38.8 ± 1.0	32.0	53.0 ± 11.6**	2.6	1.2 ± 0.2**	15.6 ± 0.6	0.46 ± 0.01	0.80 ± 0.03**

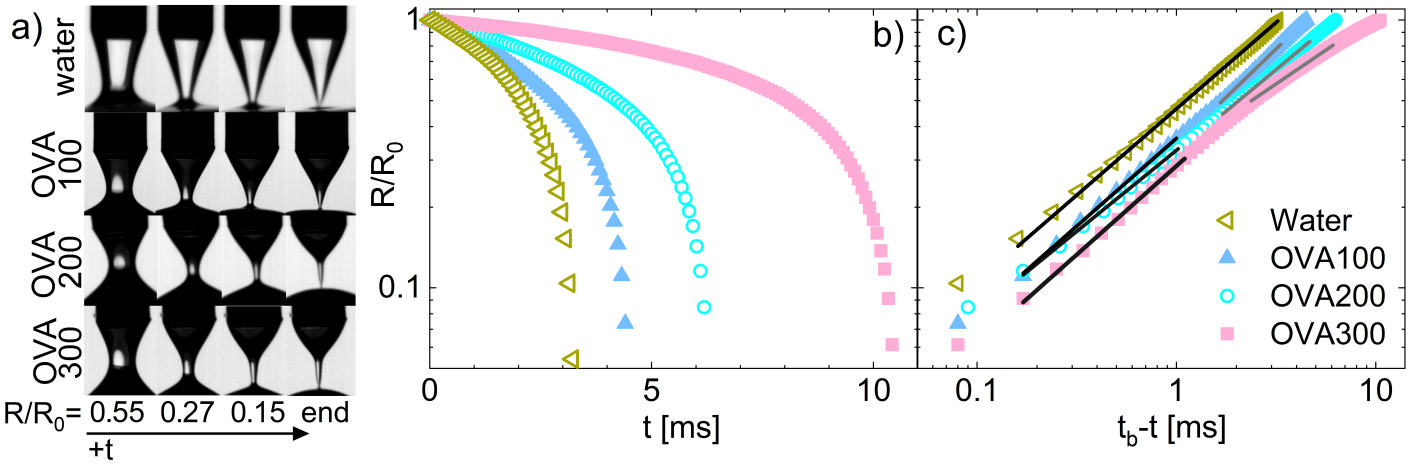

Fig. 3 a) Images during capillary thinning for water and OVA at 100, 200 and 300 mg/mL at $R/R_0 = 0.55$, 0.27, 0.15 and the endpoint, and b) corresponding radial decay in time. c) Log-log plot of R/R_0 vs. $t_b - t$ (time decreases from L to R). Power law (PL) fits for n and n_0 are the black and gray lines, respectively.

profiles are much less conical than water (Fig. 3a). By OVA300, the filament that evolves in time is substantially more cylindrical and axisymmetric about the midpoint than in OVA100. The vertical asymmetry near pinch-off for water and OVA100 (Fig. 3a), however, demonstrates the need for 2D imaging, as instruments like CaBER assume axial symmetry when determining the minimum radius of the liquid bridge.

The radial decay profiles of water and dilute OVA are expected to follow the characteristic $t^{2/3}$ scaling for inertiocapillary thinning dominated by inertial and surface tension forces[67–69]:

$$\frac{R_{min}(t)}{R_0} = \alpha \left(\frac{t_b - t}{t_R} \right)^{2/3} \tag{3}$$

with breakup time, t_b and Rayleigh time, t_R. The Rayleigh time is the characteristic timescale for IC thinning phenomena in a fluid of surface tension σ and density ρ, given by $t_R = (\rho R_0^3/\sigma)^{1/2}$. The value of the constant α has been reported experimentally between 0.4 and 1.[24,32,42,70] Recent volume-of-fluid method simulations found this prefactor to be between 0.4 and 0.6, depending on experimental parameters such as viscosity and nozzle size.[71]

To determine how well Eq. 3 described OVA behavior near the end of thinning, OVA data was fit using t^n instead of $t^{2/3}$ (black lines in Fig. 3c). In Fig. 3c, data is shown on log-log scale, such that linear regions described by a power law exponent can be more easily identified. Here, we use a constant $\alpha = 0.6$, which was found to provide the best fit across experimental data (see SI.6). By rearranging Eq. 3 to group t_R as part of the constant prefactor, we also define a new prefactor as $C = 0.6\left(\frac{\sigma}{\rho R_0^3}\right)^{1/3}$. This constant C was determined both by fitting (allowing n to vary), C_{fit}, and calculation with known parameters ($n = 2/3$), C_{calc}. For all samples, values of n, C, and t_R are reported in Table 1 and extension rates are calculated in SI.11.

Fits of n yielded an approximate scaling of $t^{2/3}$ for all OVA samples (Table 1), indicating that OVA exhibits IC behavior near the end of thinning. For both water and OVA100, the calculated and fit values for C and t_R in Table 1 are in excellent agreement, suggesting that IC thinning sufficiently describes the flow behavior (Eq. 3). As all other parameters influencing t_R are nearly identical between water and OVA100, the weaker surface tension forces in OVA100 vs. water fully account for the slower thinning process, increasing the timescale for breakup by roughly one-third.

Prior to the inertiocapillary thinning regime (longer $t_b - t$ in Fig. 3c), a region with a distinct slope appears in the OVA200 solution which becomes more pronounced in OVA300. Thus in addition to fitting the exponent corresponding to the end of thinning where the IC region is typically observed (n), a power law (PL) model was also fit to this second region near the start of thinning (n_0) to quantify how the initial behavior changes with OVA concentration (Table 1). Note that this marked change in slope is not observed in OVA100 or water which can be described entirely by IC behavior; unsurprisingly $n_0 = n$ for OVA100. The initial index n_0 decreases significantly with concentration, from $n_0 = 0.64 \pm 0.02$ for OVA100 (IC behavior) to $n_0 = 0.50 \pm 0.01$ for OVA300. This change in initial thinning behavior and increase in t_b at higher OVA content cannot be fully explained by surface tension, as σ is constant between OVA200 and OVA300. Additionally, the calculated and fit values for C and t_R deviate with increasing OVA (Table 1). These differences in parameter values, paired with the statistically significant difference in n and n_0 and deviation from $t^{2/3}$ at early times in OVA300 suggest that IC thinning (Eq. 3) is insufficient to fully describe thinning in concentrated OVA.

While the exact physical meaning of the n_0 parameter is unknown, Dinic, Jimenez and Sharma observed an index of $n = 0.5$ and similar liquid bridge shapes as OVA in particle-laden printing inks,[35] noting that interplay between complex flow phenomena may lead to a difference in n determined by DoS and shear rheology. These inks have similar flow properties to many protein solutions in that they have low viscosities, nearly-Newtonian shear behavior, and surface tensions comparable to those in Table 1.[35] Further, Brust and co-workers found significant elasticity and non-Newtonian behavior in blood plasma during capillary thinning extensional flow, whereas Newtonian behavior was observed under shear.[22] As high concentration solutions of globular OVA may have microstructures resembling these suspensions, the

decreasing n_0 with increasing OVA content may reflect the underlying microstructure or non-Newtonian behavior. Importantly, gravitational effects are not expected to be significant in the n_0 fitting range (SI.1). Analysis of this initial thinning region may thus provide further insight into the processes driving thinning and breakup of concentrated proteins that cannot be described purely by IC behavior.

Additionally, the clear IC thinning behavior at the end of thinning for all OVA solutions suggests that while OVA does lower the surface tension, the concentration-dependent differences in rheology are unlikely to be driven primarily by a protein film or surface layer. In the event of film formation, signs of weakly elastic or EC thinning behavior would be expected near the end of thinning, as opposed to clear and reproducible IC behavior. Note that OVA adsorbs to the interface slowly, such that large decreases in σ associated with adsorption occur on timescales longer ($> 10^2$ s)[20] than that required to produce the droplet and perform the capillary thinning measurement. This finding is also in agreement with prior work on a slightly larger protein from the same family, BSA, where the authors excluded surface film formation as a substantial contributor to the measured rheology.[22] Further, if the observed changes in n_0 with increasing concentration were driven by an interfacial layer rather than bulk behavior, a nearly concentration-independent n_0 would be expected, as was demonstrated in interfacially-dominated shear measurements on BSA solutions over a wide concentration range (10–250 mg/mL).[31] Instead, we suspect that the observed concentration-dependent initial thinning index reflects the concentration-dependent rheological behavior expected for colloidal suspensions.

Despite the high protein concentration in OVA300, ultimately OVA breaks apart rapidly on a timescale that is within three-fold that of the water breakup time. The maximum extension rates experienced by OVA solutions are of order 10^4 s^{-1}, corresponding well to extension rates during clinical injections (see SI.11).[5] This finding is seemingly promising for developing injectable protein medications, as the protein is unlikely to experience high extension rates that could cause denaturing for long durations. While shear rheological properties often cannot predict extensional flow behavior (and vice versa), that the OVA breakup timescale is similar to that of water suggests the absence of significant antagonistic protein-protein interactions that could increase viscosity during flow, which would hinder injectability given the formulation guidelines of $\leq$50 cP (50x viscosity of water) for subcutaneous injections.[9]

3.2 Breakup behavior of excipient poloxamer 188 (P188)

Solutions containing the excipient P188 exhibit more pronounced break up behaviors than seen in OVA solutions for equivalent weight fractions (Fig. 4a). The most dilute concentration of P188 (50 mg/mL, denoted P188-50) thins on a time scale comparable to OVA100, which contains twice the concentration of material (100 mg/mL, Fig. 4b). The 2D images of these two solutions during thinning also share nearly identical features (Fig. 4a), suggesting that they exhibit similar thinning regimes.

While P188-100 shares similar 2D thinning profiles to the P188-50 solution, increasing the concentration to 200 mg/mL P188 (P188-200) results in substantially more cylindrical filaments and a breakup time of nearly 10 ms (Fig. 4a). The slenderness of the filament near breakup increases with P188 concentration, which may be indicative of the onset of weakly elastic thinning behavior as opposed to purely IC behavior.[65,72] However, while P188 filaments are more slender the conical water filament, the thinning does not exhibit pronounced elastocapillary behavior nor a long lasting filament like in PEO solutions (Fig. 2).

Despite containing half the amount of material as in OVA100, the surface tension of P188-50 is lower (43.2 $\pm$ 0.7 mN/m vs. 47.5 $\pm$ 1.3 mN/m for OVA100). P188 may reduce the surface tension more efficiently than OVA due to its flexible conformation: despite that OVA is over five-fold greater in molecular weight than P188, its hydrodynamic radius R_h is only slightly larger due to its rigid conformation (2.9 nm vs. 2.7 nm for P188, see SI.5). Thus if both species had an equal affinity for the air-water interface, P188 would still be able to cover more of the interface than OVA, even at half the concentration. The surface of the droplet appears nearly saturated by P188-50, as the surface tension only slightly decreases to 41.4 $\pm$ 0.4 mN/m when the P188 content is doubled (P188-100); no further decrease in surface tension is observed with increasing P188 content above P188-100.

As done for OVA solutions, the end thinning behavior of P188 solutions was fit with a power law model to determine the dominant flow regimes. Lower P188 content solutions (P188-50, P188-100) exhibit inertiocapillary thinning, where values of n and n_0 are not statistically different, and are near the expected value of 2/3 for IC thinning (Table 1). The longer breakup time in P188-100 (5.8 $\pm$ 0.5 ms) vs. P188-50 (4.6 $\pm$ 0.1 ms) can be explained by the lower surface tension in P188-100. By P188 concentrations of 200 mg/mL, however, two regions of distinct slope are observed in the log-log representation of the data (Fig. 4c). Similar to the trends observed in concentrated OVA, larger deviations in the fit and calculated C and t_R are observed in P188-200. Additionally, the breakup time dramatically increases (9.6 $\pm$ 0.5 ms), and an increase in thinning index to $n = 0.77 \pm 0.02$ is observed near breakup. This change in breakup behavior in P188-200 cannot be accounted for by surface tension, as P188-100 and P188-200 have equal σ. Additionally, the PL fit for n poorly describes the last several data points, which exhibit notable curvature in the log-log representation of the data (Figs. 4c, S11).

Decay scalings greater than $t^{2/3}$ can indicate the presence of more viscous forces,[72,73] as radial thinning for a viscocapillary (VC) fluid instead scales with t. However here, Ohnesorge numbers are far below unity ($Oh \ll 1$, Eq. 1), such that VC thinning is not expected (see SI.1). As shown by Dinic et al.,[72] while filament thinning data can be fit with a power law scaling, the filament shape profile and fit of the model just before break-up should be considered when determining the proper fitting regime in order to meaningfully interpret the data. In P188-200, the slender filament profile observed near break-up combined with the poorer PL fit near the end of thinning indicates that PL and VC thinning may not adequately describe the fluid behavior (SI.7). However, the slender filament shape is characteristic of the onset of weakly elastic response,[65,72] which is unsurprising given the viscoelastic

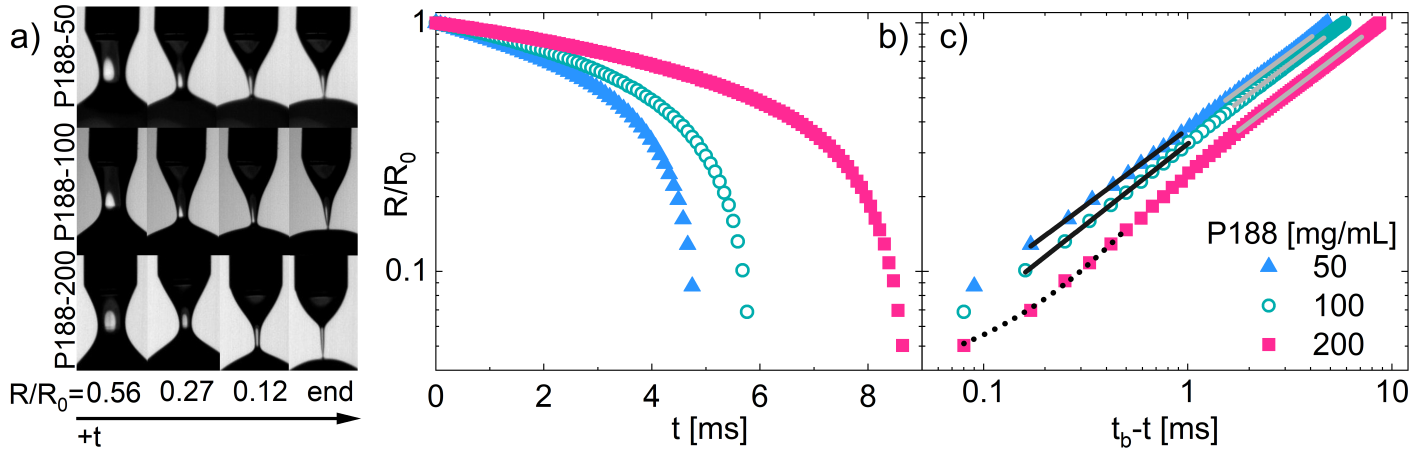

Fig. 4 a) Images during capillary thinning for 50, 100, and 200 mg/mL P188 at $R/R_0 = 0.56$, 0.27, 0.12, and the endpoint, and b) corresponding radial decay in time. c) Log-log plot of R/R_0 vs. $t_b - t$. Power law (PL) fits for n and n_0 are the black and gray lines, respectively. Anna-McKinley fit is shown in the black dashed line.

nature of poloxamer solutions.[74,75] Weakly elastic thinning behavior can be fit using the semi-empirical Anna-McKinley model, previously demonstrated to fit short duration viscoelastic behavior.[65,72] The Anna-McKinley model is given by:[65]

$$\frac{R_{min}(t)}{R_0} = A\exp(-Bt) - Ct + D \quad (4)$$

where an extensional relaxation time λ_E can be obtained from the coefficient B, given by $B \approx 1/3\lambda_E$. The coefficient C can be used to extract the terminal extensional viscosity, η_E^∞, where $C \approx \sigma/2\eta_E^\infty R_0$. Finally, the ratio of C to D gives the elastic filament lifetime, $t_E = D/C$. For P188-200 in Fig. 4b and c, t_E marks the transition in the last few milliseconds of thinning where the slope abruptly changes as weakly elastic forces dominate. The Anna McKinley model describes the behavior near break-up for P188-200 better than fits with a PL model (Figs. 4c, S11). From Eq. 4 and associated coefficients, an extensional relaxation time corresponding to the longest relaxation time of P188-200 of $\lambda_E = 0.84 \pm 0.03$ ms and elastic filament life time of $t_E = 2.0 \pm 0.3$ ms are obtained, indicating short-duration viscoelastic effects (Table 2).

3.3 Impact of added P188 on OVA extensional flow behavior

To determine the role of added excipients on OVA thinning, increasing quantities of P188 were added to a fixed OVA concentration, of 100 mg/mL (Fig. 5). Interestingly, adding 50 mg/mL of P188 to OVA100 (denoted OVA100/P188-50) yields a breakup time of $t_b = 4.8 \pm 0.3$ ms, which is remarkably similar to that of the individual constituents, OVA100 (4.4 ± 0.3 ms) and P188-50 (4.6 ± 0.1 ms; see Table 1). Like the individual component solutions, the OVA100/P188-50 solution exhibits IC thinning, with an $n = 0.66 \pm 0.02$. However, this similar breakup behavior can be attributed to surface tension: OVA100/P188-50 and P188-50 have surface tensions that are identical within statistical certainty (42.8 ± 1.5 mN/m vs. 43.2 ± 0.7 mN/m, respectively), leading to breakup times that are identical within statistical certainty. However, the similar breakup time of the combined solution despite the increasing solids volume suggests that P188 and OVA behave synergistically in some manner, as no additional reduction in surface tension is observed despite that surface tension decreases with increasing concentration in P188-only and OVA-only solutions (Table 1). The similar behavior between P188-50 and OVA100/P188-50 may suggest that P188 primarily occupies the interface and reduces the surface tension, in line with prior studies showing P188 decreases protein adsorption to interfaces, even when its affinity for the interface is low.[48,49,76,77]

The 2D images of the two protein/excipient solutions with lower P188 contents (50, 100 mg/mL) share features similar to those of their individual components (Fig. 5a). The power law fits of these combined solutions immediately prior to breakup show an exponent of roughly $n = 2/3$, characteristic of IC thinning (Fig. 5c). However, any synergistic behavior appears to vanish with increasing P188 content, as OVA100/P188-100 has a longer break-up time than either OVA or P188 alone when compared at equivalent σ (t_b=7.3 ± 0.3 ms). For example, OVA200 and OVA100/P188-100 both have surface tensions of 42.1 mN/m, but the breakup time in the combined OVA/P188 solution is 20% longer. Additionally, while calculated and fit C and t_R agreed well for OVA100/P188-50, substantial deviations are observed in OVA100/P188-100. Here, the calculated C-value is substantially higher while the calculated t_R is lower, similar to the trend observed with increasing OVA content when a second power law

Table 2 The weakly elastic samples were fit with the Anna-McKinley model to obtain the extensional relaxation time λ_E, terminal extensional viscosity η_E^∞, and elastic time. Reported uncertainty is the 95% confidence interval of the parameter value based on fits to all trials.

sample	λ_E [ms]	η_E^∞ [Pa · s]	t_E [ms]
P188-200	0.84 ± 0.03	0.37 ± 0.02	2.0 ± 0.3
OVA100/P188-200	1.1 ± 0.1	0.56 ± 0.06	3.6 ±0.1
OVA200/P188-100	1.2 ± 0.1	0.38 ± 0.03	2.6 ± 0.2

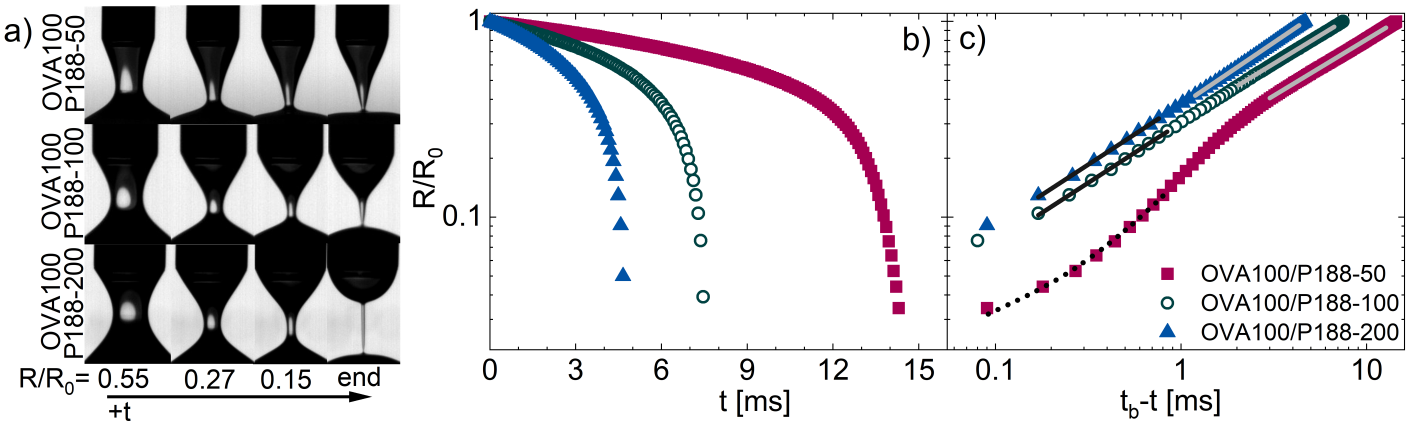

Fig. 5 a) Images during capillary thinning for 100 mg/mL OVA with P188 added at 50, 100, and 200 mg/mL for $R/R_0 = 0.55$, 0.27, 0.15 and the endpoint, and b) corresponding radial decay in time. c) Log-log plot of R/R_0 vs. $t_b - t$. Power law (PL) fits for n and n_0 are the black and gray lines, respectively. Anna-McKinley fit is shown in the black dashed line.

region appeared in the log-log representation of the data (Table 1, Fig. 3c). Unsurprisingly, a lower thinning index is observed initially vs. near the end of thinning ($n_0 = 0.58 \pm 0.02$ vs. $n = 0.65 \pm 0.02$), suggesting that IC thinning does not fully describe the phenomena in OVA100/P188-100.

Potential antagonistic effects appear to amplify at the highest P188 concentration, OVA100/P188-200. This solution has a break-up time (14.9 ± 1.3 ms) that is statistically equal to the sum of its individual components (14.0 ± 0.6 ms), unlike in OVA100/P188-50 where the breakup time was similar to that of a single component. While this solution has the lowest surface tension of all samples (37.7 ± 2.0 mN/m), the shape of the radial decay data (Fig. 5c), the drastic differences in calculated and fit values for C and t_R (Table 1), and deviations from PL fits (Fig. S12) clearly suggest flow behaviors beyond IC and PL thinning. Additionally, the 2D images of the radial decay display features not present in either of the individual components. In particular, this concentrated OVA/P188 solution shows thinning profiles far more slender and axisymmetric prior to breakup than any other P188 or OVA solution examined (Fig. 5a), reminiscent of the weakly elastic thinning behavior observed in P188-200. Using the Anna-McKinley model (Eq. 4), the extensional relaxation time for OVA100/P188-200 is $\lambda_E = 1.1 \pm 0.1$ ms. Here, λ_E is 30% longer and t_E is 80% longer than in P188-200, which is unsurprising given the substantially more pronounced elastic-like features in the 2D images (Fig. 5a).

3.4 Role of total concentration on observed flow behavior

The longer extensional relaxation time in OVA100/P188-200 vs. P188-200 alone is perhaps unsurprising given the higher total concentration in solution (300 mg/mL) when OVA is added. However, no notable elasticity was observed at 300 mg/mL OVA, suggesting a minimum P188 and total concentration may be required to observe weakly elastic behavior. An additional concentrated solution containing 200 mg/mL OVA and 100 mg/mL P188 (OVA200/P188-100) was thus examined to confirm this hypothesis. This formulation was chosen to keep a constant total concentration (300 mg/mL) while examining a P188 concentration (100 mg/mL) at which other solutions did not exhibit weak elasticity (P188-100, OVA100/P188-100). While no statistically significant difference in surface tension is observed between the formulations containing P188, OVA300 does exhibit a slightly higher σ, which is unsurprising based on the prior DoS results showing that P188 more efficiently reduces σ than OVA (Table 1).

Despite containing a lower P188 content, the 2D images and radial decay profiles for OVA200/P188-100 suggest similar thinning and elastic-like behavior to OVA100/P188-200 (Fig. 6). As shown in Fig. 6b and reported in Table 1, representative trials for both protein/excipient solutions exhibit similar breakup times; parameters extracted from the Anna-McKinley model are compared in Table 2. However, notable differences are present between the two protein/excipient solutions, where images in Fig. 6a suggest that the cylindrical filament forms earlier and is more slender in the formulation containing more P188 (OVA100/P188-200). That the filament appears more pronounced in the presence of more P188 is supported by differences in the shape of the radial decay near breakup (Fig. S14a) and values of the elastic filament lifetime t_E extracted from the Anna-McKinley fit: t_E is ~40% longer in OVA100/P188-200. Additionally, the terminal extensional viscosity η_E^∞ is roughly 50% larger in the solution containing more P188 (OVA100/P188-200); see SI.8 for a more detailed comparison of Anna-McKinley model fits and fitting ranges for all samples displaying weakly elastic behavior. Despite the shorter filament lifetime, the extensional relaxation times are identical within statistical certainty for the 300 mg/mL protein/excipient formulations, and are longer than in P188-200 (Table 2); this finding suggests that while P188 is required to observe weakly elastic thinning, the high total solution concentration also contributes to the observed elasticity.

Interestingly, the formulation containing less excipient (OVA200/P188-100) exhibits a substantially lower initial thinning index, where $n_0 = 0.46 \pm 0.01$ vs. $n_0 = 0.56 \pm 0.03$ for OVA100/P188-200. This feature is noticeable when the data is observed on a log-log scaling (Fig. 6c), where the linear regions of the data corresponding to the beginning of thinning (long $t - t_b$) clearly intersect one another due to this difference in n_0. This reduction in n_0 likely results from the increased OVA con-

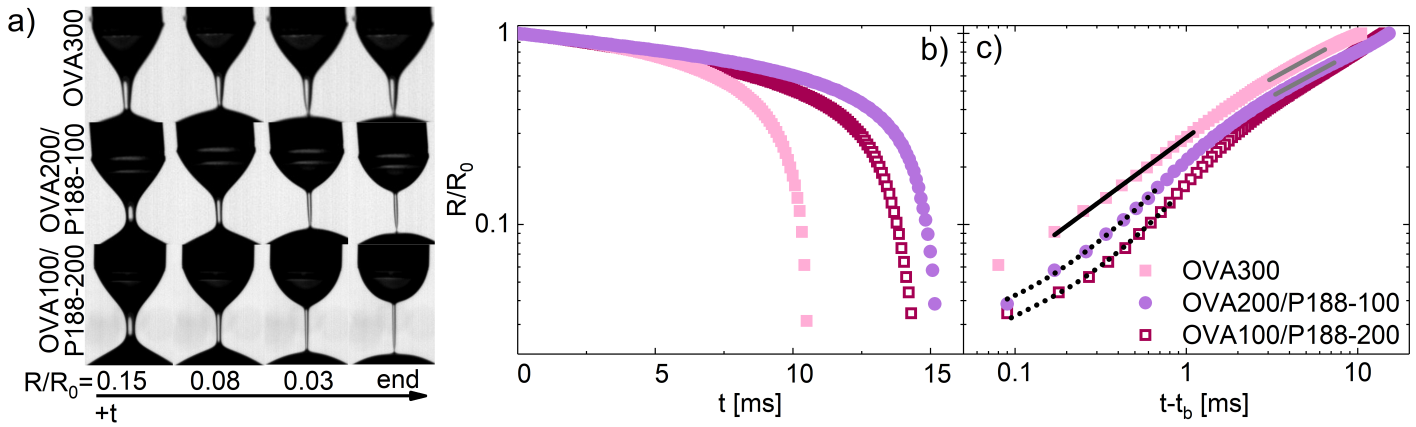

Fig. 6 a) Images of capillary thinning in concentrated formulations: 300 mg/mL OVA, OVA200/P188-100 and OVA100/P188-200, at $R/R_0 = 0.15$, 0.08, 0.03 and the endpoint, and b) corresponding radial decay in time. c) Log-log plot of R/R_0 vs. $t_b - t$. Fits used to extract n and n_0 are shown in black and gray, respectively. The Anna-McKinley fits are shown with dashed black lines.

tent, as OVA-only solutions saw n_0 continually decrease with increasing concentration whereas the n_0 in P188 solutions appeared independent of concentration (Table 1). Thus despite that the elastic filament time is shorter for OVA200/P188-100, t_b appears to be equal between samples or slightly larger for this sample (15.6 ± 0.6 ms for OVA200/P188-100 vs. 14.9 ± 1.3 ms for OVA100/P188-200) because the initial thinning process proceeds more slowly.

3.5 Rationalizing observed flow behavior

A clear, weakly elastic thinning regime emerges in both high concentration protein/excipient solutions, a consequence of both the high solution concentration and the extensibility of the P188 chain. We suspect that both criteria must be met to observe this behavior, as the equally concentrated 300 mg/mL OVA does not exhibit signatures of elasticity during breakup, whereas solutions containing P188-200 also exhibit weakly elastic behavior, albeit less pronounced. Similar to observations by Brust and coworkers,[22] we do not expect an OVA surface layer to be driving the observed elasticity in formulations of 300 mg/mL protein/excipient, both because P188 addition is thought to reduce OVA coverage[48,49,76,77] and associated elasticity[31,78] at the interface, and because no elastic effects are observed during thinning in OVA300. In addition to altering protein conformation, crowded solution environments can alter excluded volume and dipole-dipole interactions[21]; these effects could help explain the emergence of a second PL region in concentrated OVA. However, as concentrated OVA does not exhibit weakly elastic thinning behavior, we conclude that the observed elasticity is driven by P188.

Chain extensibility effects in P188 are expected to be more pronounced prior to micellization, as the hydrodynamic volume per unimer decreases with micellization and subsequently decreases related quantities like shear viscosity.[79] All solutions containing P188 likely had a high fraction of P188 unimers, even at high P188 concentrations like in the combined OVA100/P188-200 solution. The critical micelle temperature (CMT) of P188 is substantially higher than for most other poloxamers, reported as 27 °C at 150 mg/mL[74]; this high CMT is a result of the high fraction of hydrophilic PEO in P188 (80% wt). As our measurements at room temperature (23 ± 0.5 °C) are below the CMT for 150 mg/mL P188, the solutions between 10 and 100 mg/mL P188 likely contain solely unimers. This finding is supported by DLS measurements of P188 in water (SI.5). At and below 100 mg/mL P188, the hydrodynamic radius, R_h, is ∼2.5 nm, which correlates well with the reported P188 unimer size.[80] Here, DLS data is described well by a single population; no evidence of micelle formation (∼7 nm[80]) is observed.

Across all DoS formulations, the presence of P188 unimers enhances the elasticity and breakup time of the solutions. For P188 and OVA solutions of the same concentration, P188 solutions have breakup times that are 30-50% longer in duration. The P188-200 and OVA100/P188-200 solutions likely contain a mix of micelles and unimers, as extrapolating previous data[74] to higher P188 concentrations suggests that the onset of micellization may occur by 24 °C for solutions containing 200 mg/mL P188; however, poloxamers are known to exhibit micellization transitions over temperatures range of 10 °C or more[74,75,81] due to their high polydispersity.

The onset of weakly elastic behavior can be detected by analyzing the 2D images during thinning and by examining deviations in the power law model fits to the 1D radial decay profiles (SI.7). In P188 solutions, a dramatic change in liquid bridge shape from conical (P188-100) to cylindrical (P188-200) occurs (Fig. 4), which is expected when new thinning regimes are accessed[35,72]; thus the onset of weakly viscoelastic behavior likely occurs between P188-100 and P188-200. These shape changes also identify radial decay regimes in which the power law model is inappropriate, justifying fitting concentrated P188 data with the Anna-McKinley model as recently detailed by Dinic and Sharma.[65,72] Additionally, we find that comparing the fit and calculated values of C and t_R is useful in differentiating between weakly elastic and PL behavior (Table 1). When a second PL region emerges in the data like in concentrated OVA, C_{calc} exceeds C_{fit} whereas $t_{R,calc}$ falls below $t_{R,fit}$; however, n remains near $n \approx 2/3$. However for formulations exhibiting weakly elastic behavior (P188-200, OVA100/P188-200 and OVA200/P188-100), n substantially increases and trends with respect to C and

t_R reverse: C_{calc} falls below C_{fit} whereas $t_{R,calc}$ exceeds $t_{R,fit}$.

Excipient assembly and associations with proteins depend on excipient type and concentration. As seen in the 300 mg/mL OVA/P188 solutions, adding P188 to concentrated formulations results in enhanced stretching, which is not substantially reduced even when OVA is the majority component; additional studies are needed to determine the maximum P188 loadings and/or total concentrations that can be used without promoting weakly elastic behavior. Despite promoting this undesirable flow behavior in concentrated formulations, P188 behaves synergistically with OVA at the lowest P188 content, indicating that P188 may stabilize OVA solutions under both shear and extensional flows for more dilute formulations. These findings are supported by recent work of Rodrigues et al.,[21] who showed that excipients that performed best in lowering viscosity and improving formulation concentratability in low to moderately concentrated proteins performed the worst with respect to these metrics at ultra-high concentrations (>150 mg/mL). The authors concluded that protein-excipient interactions are not only protein-specific, but also protein-concentration specific, in agreement with our conclusions.

Though several mechanisms of interaction between OVA and P188 have been proposed,[49,76,82] a number of studies show that P188 prevents OVA from adsorbing to the droplet interface.[48,49,76,77] The protein and unimer hydrodynamic radii are similar in size, and the absence of multiple populations in the DLS data suggests the absence of large protein-poloxamer complexes. However, the emergence of weakly elastic behavior with increasing P188 content and disappearance of the protective effect at high P188 content suggests that any synergistic behaviors, like P188 preventing OVA adsorption at the interface, may saturate at high P188 content. In this event, free P188 unimers in solution could lead to enhanced stretching in the most concentrated solutions. Thus if added in sufficiently large quantities or in highly concentrated solutions, excipients added to prevent protein aggregation at rest and under shear flow may lead to undesirable enhanced elasticity and stretching in extensional flow, depending on the specific excipient properties and mode of interaction with the protein.

4 Conclusions

We developed and validated a direct-mount dripping-onto-substrate (DoS) device to enable measurement of extensional flow behavior of dilute through concentrated solutions of macromolecules like proteins and polymers in less than 10 μL total per trial. By developing a 'stationary drop' method to perform DoS measurements, vibrations and instabilities that highly impact dilute solution thinning are minimized, and the surface tension can be extracted as part of the measurement to aid in data analysis. Despite the low viscosities of protein and excipient solutions, all solutions studied demonstrated distinct thinning behavior from water, largely driven by lower surface tension forces for low protein and excipient concentrations. Break-up times for OVA solutions increase with concentration, though this behavior cannot be attributed entirely to inertiocapillary thinning at the highest OVA concentrations. Despite these deviations from IC thinning, concentrated OVA solutions still break apart rapidly. These findings are ultimately promising for developing concentrated injectable protein medications of similar size to OVA, as pure OVA solutions exhibit no signatures of elastic-like behavior in extension.

The excipient P188 exhibited longer break up times at equivalent concentrations to OVA, and surface tension comparisons suggest that these differences can largely be attributed to P188 more effectively reducing σ. However, the 2D thinning profiles of concentrated P188 exhibited more cylindrical shapes and longer break up times, corresponding to appearance of weakly elastic behavior with increasing P188 content. At the concentrations studied, all P188 solutions likely have P188 unimers present, thereby increasing elasticity. At low P188 content, combined OVA/P188 solutions exhibit synergistic behavior, where the breakup times reflect the reduced surface tension. The measured surface tension reflects the P188 content, in agreement with prior findings that P188 prevents OVA migration to the interface; these results suggest that P188 has a protective effect in extension in addition to shear at lower P188 content. However in the highest concentration protein/excipient solutions, thinning profiles are far more cylindrical than observed in other formulations, indicating emergence of weakly elastic flow behavior. These concentrated 300 mg/mL OVA/P188 solutions are well-described by the Anna-McKinley model for weakly elastic fluids, where the elastic filament lifetime and terminal extensional viscosity increase with P188 content. These findings suggest that while P188 is beneficial for stabilizing OVA solutions when added to dilute formulations, the presence of P188 in increasingly concentrated solutions can lead to undesirable elasticity during extensional flows.

Author Contributions

A.L.R. performed DLS experiments and surface tension measurements; K.T.L. carried out all other experiments including DoS, SDS-PAGE, and additional DLS and surface tension measurements. K.T.L. performed data fits and wrote the manuscript with assistance from M.A.C.

Conflicts of interest

The authors declare no competing interests.

Acknowledgements

This material is based upon work supported by the National Science Foundation Graduate Research Fellowship under Grant No. CON-75851, project 00074041. Any opinions, findings, and conclusions or recommendations expressed in this material are those of the author(s) and do not necessarily reflect the views of the National Science Foundation. The authors thank the Anton Paar VIP program for the shear rheometer used in this work, and Kristen Lemke and Joseph Vallin for assistance with SDS-PAGE.

Notes and references

1 W. Wang, S. Singh, D. L. Zeng, K. King and S. Nema, *J. Pharm. Sci.*, 2007, **96**, 1–26.

2 E. Moorkens, N. Meuwissen, I. Huys, P. Declerck, A. G. Vulto and S. Simoens, *Front. Pharmacol.*, 2017, **8**, 314.

3 J. L. Mann, C. L. Maikawa, A. A. Smith, A. K. Grosskopf, S. W.

Baker, G. A. Roth, C. M. Meis, E. C. Gale, C. S. Liong, S. Correa *et al.*, *Science Trans. Med.*, 2020, **12**, 6676.
4 L. M. Marquardt, V. M. Doulames, A. T. Wang, K. Dubbin, R. A. Suhar, M. J. Kratochvil, Z. A. Medress, G. W. Plant and S. C. Heilshorn, *Science Adv.*, 2020, **6**, eaaz1039.
5 I. B. Bekard, P. Asimakis, J. Bertolini and D. E. Dunstan, *Biopolymers*, 2011, **95**, 733–745.
6 Z. Zhang and Y. Liu, *Curr. Opin. Chem. Eng.*, 2017, **16**, 48–55.
7 J. Liu, M. D. Nguyen, J. D. Andya and S. J. Shire, *J. Pharm. Sci.*, 2005, **94**, 1928–1940.
8 L. Jovanovic-Peterson, S. Sparks, J. P. Palmer and C. M. Peterson, *Diabetes Care*, 1993, **16**, 1479–1484.
9 M. A. Miller, J. D. Engstrom, B. S. Ludher and K. P. Johnston, *Langmuir*, 2009, **26**, 1067–1074.
10 J. Jezek, M. Rides, B. Derham, J. Moore, E. Cerasoli, R. Simler and B. Perez-Ramirez, *Adv. Drug Delivery Rev.*, 2011, **63**, 1107–1117.
11 N. Rathore, P. Pranay, J. Bernacki, B. Eu, W. Ji and E. Walls, *J. Pharm. Sci.*, 2012, **101**, 4472–4480.
12 W. Wang, S. Nema and D. Teagarden, *Int. J. Pharm.*, 2010, **390**, 89–99.
13 M. M. Castellanos, J. A. Pathak and R. H. Colby, *Soft Matter*, 2014, **10**, 122–131.
14 Y.-F. Maa and C. C. Hsu, *Biotechnol. Bioeng.*, 1997, **54**, 503–512.
15 S. Simon, H. Krause, C. Weber and W. Peukert, *Biotechnol. Bioeng.*, 2011, **108**, 2914–2922.
16 D. Nesta, T. Nanda, J. He, M. Haas, S. Shpungin, I. Rusanov, R. Sweder and C. Brisbane, *Bioprocess Int.*, 2017, **15**, 30–39.
17 L. Nicoud, M. Owczarz, P. Arosio and M. Morbidelli, *Biotechnol. J.*, 2015, **10**, 367–378.
18 J. S. Horner, A. N. Beris, D. S. Woulfe and N. J. Wagner, *Clin. Hemorheol. Microcirc.*, 2018, **70**, 155–172.
19 P. Dhar, Y. Cao, T. M. Fischer and J. A. Zasadzinski, *Phys. Rev. Lett.*, 2010, **104**, 016001.
20 A. H. Martin, K. Grolle, M. A. Bos, M. A. C. Stuart and T. van Vliet, *Journal of Colloid and Interface Science*, 2002, **254**, 175–183.
21 D. Rodrigues, L. M. Tanenbaum, R. Thirumangalathu, S. Somani, K. Zhang, V. Kumar, K. Amin and S. V. Thakkar, *J. Pharm. Sci.*, 2021, **110**, 1077–1082.
22 M. Brust, C. Schaefer, R. Doerr, L. Pan, M. Garcia, P. Arratia and C. Wagner, *Phys. Rev. Lett.*, 2013, **110**, 078305.
23 V. Sharma, S. J. Haward, J. Serdy, B. Keshavarz, A. Soderlund, P. Threlfall-Holmes and G. H. McKinley, *Soft Matter*, 2015, **11**, 3251–3270.
24 G. H. McKinley, *Rheology Reviews*, 2005, **05-P-04**, 1–50.
25 C. E. Sing and A. Alexander-Katz, *Biophys. J.*, 2010, **98**, L35–L37.
26 S. Rammensee, U. Slotta, T. Scheibel and A. Bausch, *Proc. Natl. Acad. Sci.*, 2008, **105**, 6590–6595.
27 J. Dobson, A. Kumar, L. F. Willis, R. Tuma, D. R. Higazi, R. Turner, D. C. Lowe, A. E. Ashcroft, S. E. Radford, N. Kapur and D. J. Brockwell, *Proc. Natl. Acad. Sci.*, 2017, **114**, 4673–4678.
28 L. F. Willis, A. Kumar, J. Dobson, N. J. Bond, D. Lowe, R. Turner, S. E. Radford, N. Kapur and D. J. Brockwell, *Biotechnol. Bioeng.*, 2018, **115**, 1216–1225.
29 H. Hosseini, A. Rangchian, M. Prins, C. Giza, J. Ruberti and H. Kavehpour, *J. Biomech. Eng.*, 2020, **142**, 034501.
30 A. Allmendinger, S. Fischer, J. Huwyler, H.-C. Mahler, E. Schwarb, I. E. Zarraga and R. Mueller, *Eur. J. Pharm. Biopharm.*, 2014, **87**, 318–328.
31 V. Sharma, A. Jaishankar, Y.-C. Wang and G. H. McKinley, *Soft matter*, 2011, **7**, 5150–5160.
32 J. Dinic, Y. Zhang, L. N. Jimenez and V. Sharma, *ACS Macro Lett.*, 2015, **4**, 804–808.
33 M. Renardy, *J. Non-Newton Fluid*, 1995, **59**, 267–282.
34 J. Dinic and V. Sharma, *Proc. Natl. Acad. Sci.*, 2019, **116**, 8766–8774.
35 J. Dinic, L. N. Jimenez and V. Sharma, *Lab Chip*, 2017, **17**, 460–473.
36 E. Miller, C. Clasen and J. P. Rothstein, *Rheol. Acta*, 2009, **48**, 625–639.
37 L. E. Rodd, T. P. Scott, J. J. Cooper-White and G. H. McKinley, *Appl. Rheol.*, 2005, **15**, 12–27.
38 S. Wu and H. Mohammadigoushki, *J. Rheol.*, 2018, **62**, 1061–1069.
39 S. Sur and J. Rothstein, *J. Rheol.*, 2018, **62**, 1245–1259.
40 K. A. Marshall and T. W. Walker, *Rheol. Acta*, 2019, **58**, 573–590.
41 C. D. M. Narváez, T. Mazur and V. Sharma, *Soft Matter*, 2021.
42 M. Rosello, S. Sur, B. Barbet and J. Rothstein, *J. Non-Newton Fluid*, 2019.
43 L. N. Jimenez, C. D. M. Narváez, C. Xu, S. Bacchi and V. Sharma, *Soft Matter*, 2021, **17**, 5197–5213.
44 T. Wang, A. Markham, S. J. Thomas, N. Wang, L. Huang, M. Clemens and N. Rajagopalan, *J. Pharm. Sci.*, 2019, **108**, 1264–1271.
45 Y. Zhu, J.-X. Xu, J. Cheng, Z. Zhang, B.-Q. Zhu, T.-Y. Chen, X.-Y. Xu, Y. Wang, M.-Y. Cai and P.-H. Zhou, *United Eur. Gastroent.*, 2019, **7**, 782–789.
46 J. G Moloughney and N. Weisleder, *Recent Pat. Biotechnol.*, 2012, **6**, 200–211.
47 D. Mustafi, C. M. Smith, M. W. Makinen and R. C. Lee, *Biochim. Biophys. Acta*, 2008, **1780**, 7–15.
48 C. Grapentin, C. Müller, R. S. Kishore, M. Adler, I. ElBialy, W. Friess, J. Huwyler and T. A. Khan, *J. Pharm. Sci.*, 2020, **109**, 2393–2404.
49 S. Dubey and R. Giovannini, *Trends Biotechnol.*, 2020, 546–549.
50 C. Beck, M. Grimaldo, F. Roosen-Runge, M. K. Braun, F. Zhang, F. Schreiber and T. Seydel, *J. Phys. Chem. B*, 2018, **122**, 8343–8350.
51 T. J. Kamerzell, R. Esfandiary, S. B. Joshi, C. R. Middaugh and D. B. Volkin, *Adv. Drug Deliv. Rev.*, 2011, **63**, 1118–1159.
52 A. Paillard-Giteau, V.-T. Tran, O. Thomas, X. Garric, J. Coudane, S. Marchal, I. Chourpa, J.-P. Benoît, C. Montero-

Menei and M.-C. Venier-Julienne, *Eur. J. Pharm. Biopharm.*, 2010, **75**, 128–136.
53 L. Seta, N. Baldino, D. Gabriele, F. R. Lupi and B. de Cindio, *Food Hydrocoll.*, 2012, **29**, 247–257.
54 J. Wiesbauer, R. Prassl and B. Nidetzky, *Langmuir*, 2013, **29**, 15240–15250.
55 U. K. Laemmli, *Nature*, 1970, **227**, 680–685.
56 Y.-T. Xu, Y.-H. Wang, F.-P. Chen and C.-H. Tang, *Food Hydrocoll.*, 2020, **103**, 105694.
57 J. Liu, J. Liu and X. Zhang, *Int. J. Food Eng.*, 2012, **8**, 1–12.
58 C. A. Schneider, W. S. Rasband and K. W. Eliceiri, *Nat. Methods*, 2012, **9**, 671.
59 A. M. Daeer, A., *J. Open Res. Softw.*, 2016, **4**, e3.
60 N. Vargaftik, B. Volkov and L. Voljak, *J. Phys. Chem. Ref. Data*, 1983, **12**, 817–820.
61 A. Rajappan and G. H. McKinley, *Sci. Rep.*, 2019, **9**, 1–14.
62 W. Mathues, S. Formenti, C. McIlroy, O. G. Harlen and C. Clasen, *J. Rheol.*, 2018, **62**, 1135–1153.
63 J. Dinic, M. Biagioli and V. Sharma, *J. Polym. Sci. B Polym. Phys.*, 2017, **55**, 1692–1704.
64 V. Entov and E. Hinch, *J. Non-Newton Fluid*, 1997, **72**, 31–53.
65 S. L. Anna and G. H. McKinley, *J. Rheol.*, 2001, **45**, 115–138.
66 S. Morozova, P. W. Schmidt, A. Metaxas, F. S. Bates, T. P. Lodge and C. S. Dutcher, *ACS Macro Lett.*, 2018, **7**, 347–352.
67 R. F. Day, E. J. Hinch and J. R. Lister, *Phys. Rev. Lett.*, 1998, **80**, 704.
68 J. R. Castrejón-Pita, A. A. Castrejón-Pita, E. J. Hinch, J. R. Lister and I. M. Hutchings, *Phys. Rev. E*, 2012, **86**, 015301.
69 D. H. Peregrine, G. Shoker and A. Symon, *J. Fluid Mech.*, 1990, **212**, 25–39.
70 L. Campo-Deano and C. Clasen, *J. Nonnewton. Fluid Mech.*, 2010, **165**, 1688–1699.
71 A. Deblais, M. Herrada, I. Hauner, K. P. Velikov, T. Van Roon, H. Kellay, J. Eggers and D. Bonn, *Phys. Rev. Lett.*, 2018, **121**, 254501.
72 J. Dinic and V. Sharma, *Macromolecules*, 2020, **53**, 3424–3437.
73 R. Suryo and O. A. Basaran, *J. Nonnewton. Fluid Mech.*, 2006, **138**, 134–160.
74 P. Alexandridis, J. F. Holzwarth and T. A. Hatton, *Macromolecules*, 1994, **27**, 2414–2425.
75 P. J. McCauley, S. Kumar and M. A. Calabrese, *Langmuir (accepted)*, 2021.
76 H. L. Kim, A. Mcauley, B. Livesay, W. D. Gray and J. Mcguire, *J. Pharm. Sci.*, 2014, **103**, 1043–1049.
77 H. L. Kim, A. Mcauley and J. Mcguire, *J. Pharm. Sci.*, 2014, **103**, 1337–1345.
78 T. W. Patapoff and O. Esue, *Pharm. Dev. Technol.*, 2009, **14**, 659–664.
79 P. Bahadur, K. Pandya, M. Almgren, P. Li and P. Stilbs, *Colloid Polym. Sci.*, 1993, **271**, 657–667.
80 U. Adhikari, A. Goliaei, L. Tsereteli and M. L. Berkowitz, *J. Phys. Chem. B*, 2016, **120**, 5823–5830.
81 P. Alexandridis and J. F. Holzwarth, *Langmuir*, 1997, **13**, 6074–6082.
82 H. J. Lee, A. McAuley, K. F. Schilke and J. McGuire, *Adv. Drug Delivery Rev.*, 2011, **63**, 1160–1171.